


PAPER

A smart Kevlar-based triboelectric nanogenerator with enhanced anti-impact and self-powered sensing properties

To cite this article: Fang Yuan *et al* 2020 *Smart Mater. Struct.* **29** 125007

View the [article online](#) for updates and enhancements.

A smart Kevlar-based triboelectric nanogenerator with enhanced anti-impact and self-powered sensing properties

Fang Yuan, Shuai Liu, Jianyu Zhou, Xiwen Fan, Sheng Wang and Xinglong Gong 

CAS Key Laboratory of Mechanical Behavior and Design of Materials, CAS Center for Excellence in Complex System Mechanics, Department of Modern Mechanics, University of Science and Technology of China (USTC), Hefei, Anhui 230027, People's Republic of China

E-mail: gongxl@ustc.edu.cn and wsh160@ustc.edu.cn

Received 24 May 2020, revised 7 July 2020

Accepted for publication 13 August 2020

Published 26 October 2020



CrossMark

Abstract

A novel single electrode triboelectric nanogenerator (TENG) with high energy-harvesting performance and safeguarding behavior has been developed by integrating carbon nanotubes (CNTs) and shear stiffening gel (SSG) on Kevlar fabric. The output voltage and power of the three layer structure SSG/CNTs/Kevlar-based TENG (S-TENG) reaches to as high as 41.27 V and 212.90 μ W, respectively. Due to the good triboelectric property, S-TENG also acts as a wearable self-powered device to harvest as well as monitor various human motions. More importantly, when impacted by a 1.26 kg impactor dropping from 30 cm, S-TENG with enhancing stiffness can not only resist the impact force, but also gather dynamic impact energy by producing an output voltage of 1.50 V. Finally, the mechanical and the electric properties of the S-TENG under the heavy hammer impact and quasi-static piercing has simultaneously investigated. In comparison to the neat Kevlar (7.66 J), the critical impact energy resisted by S-TENG is as high as 19.16 J, indicating a better anti-impacted property. Because of the excellent triboelectric and anti-impact properties, the smart S-TENG with self-power sensing, energy-gathering and safeguarding performance possesses high potential in next generation of body armor materials, robots, wearable electronics and human-machine interactions.

Supplementary material for this article is available [online](#)

Keywords: Kevlar fabric, shear thickening gel, anti-impact, self-powered sensing, energy harvesting

(Some figures may appear in colour only in the online journal)

1. Introduction

Triboelectric nanogenerators (TENGs), based on the coupling triboelectric effect and electrostatic induction, was a device which could convert mechanical energy into electricity [1, 2]. As a new green and sustainable power source, TENG could harvest various kinds of kinetic energies, such

as wind energy, tidal energy and bio-kinetic energy [3–6]. Owing to the easy-fabrication, environmental friendliness, high triboelectric properties, TENG showed promising applications in biomedicine [7], environment/health monitors [8–10], wearable human-interactive interfaces [11] and consumer electronics [12, 13]. In recent years, as portable electronics have been flourished as necessities in daily life, the demand

of wearable power sources was also urgently-needed. TENG showed many advantages as a flexible power system owing to its soft structures, light volume and high-efficiency in collecting energy from ambient environments [14, 15]. Without additional charging electricity, various TENG devices have been developed to power modern electronics [16, 17]. Typically, textile, as an intrinsic wearable material, was an ideal candidate substrate for novel TENGs since it was a common wearable composite. Thus, one strategy was to construct prevailing TENGs based on textiles. So far, great achievements have gained in developing novel textile-based TENG devices.

Recently, woven textile TENGs with waterproof property which could harvest various energy including human motions have been intensively studied [18, 19]. Besides the remarkable washing durability, a multifunctional textile-TENG with anti-bacterial property could simultaneously gather energy from body movements to power wearable electronics [20]. More interestingly, a stretchable electromagnetic shielding hybrid TENG, based on conductive anti-electromagnetic radiation fabric, could not only scavenge mechanical energy from living environment but also monitor human health [21]. However, the reported textile-based TENGs were mainly focused on collecting low-speed physiological motion energy while ignored to explore other high-speed impact energies under collision [22–24]. It was known dynamic impact kinetic energy were widespread in sports and even car accident. It easily caused physical discomfort, injury and property loss. Although traditional textiles could provide intrinsic protection and warm to human beings, they were easy to destruct and fail under dynamic impact excitations. Therefore, the textile-based TENG as a self-powered device to harvest dynamic impact energy, as well as protect the human body with enhanced anti-impact property was still an unsolved issue.

Kevlar, a kind of aromatic polyamide fiber, showed the wide application in body armor because of its high strength, lightweight and flexibility [25]. To meet the practical demands of next generation wearable devices in body armor, multifunctional Kevlar based protective textile devices become a key requirement. Most of the previous works were focused on the anti-impact and energy absorption properties of Kevlar-based textiles [26, 27]. Many kinds of functional materials such as ZnO nanowires, carbon nanotubes (CNTs), shear thickening fluid have been introduced into the aramid fibers to drastically enhance the impact resistance of Kevlar textiles owing to the improving of textile inter-yarn friction [28, 29]. High energy adsorption, well movement monitoring, and light weight are the three challenges in novel Kevlar based wearable body armor. So far, several wearable anti-impact piezoresistive electronic textiles which also could monitor various human body movements have been reported [30]. Unfortunately, additional power supplies were always necessary in previously Kevlar electronics. External batteries inevitably increased the weight of body armor and was also harmful to the environment. To overcome this disadvantage and further improve the anti-impact property of Kevlar fiber, one effective strategy was to introduce high friction material and design novel structure to endow the fabric with self-powered property.

Regretably, Kevlar-based TENG with enhanced mechanical property has not been reported yet.

Shear stiffening gel (SSG) is a derivative of polyboron-dimethylsiloxane. SSG is soft but it turns to rigid under high rate impact. Thus, it shows promising application in dampers and body protection [31]. Therefore, taking advantage of Kevlar fabric and SSG may design a distinctive multifunctional fabric-based TENG toward wearable self-powered sensing devices with enhanced safeguarding property. Herein, we designed a novel smart SSG/CNT/Kevlar TENG-based body armor with energy-harvesting, anti-impact, and motion sensing properties. The SSG-based TENG (S-TENG) performed good triboelectric property which generated a voltage of 41.27 V and power of 212.90 μW under the excitation of 60 N and 10 Hz. Based on the triboelectric effect, the reported smart S-TENG device could detect various human motions and detect different contacted materials. Importantly, the S-TENG device showed excellent safeguarding and energy-gathering performance compared to traditional textile TENGs and it can even storage high impact energy. Finally, the mechanical and the electric output signals of S-TENG under quasi-static piercing and harsh impact conditions were also simultaneously investigated. The fabricated self-powered flexible S-TENG could not only increase the protective property of traditional Kevlar fiber, but also settle the power supply issue of traditional body armor materials. Thus, the intelligent Kevlar based S-TENG with energy-harvesting and anti-impact property showed promising applications in next generation safeguards, wearable electronics and human-machine interactive devices.

2. Experiment section

2.1. Materials

Benzoyl peroxide (BPO), sodium dodecyl benzene sulfonate (SDBS), dimethylsiloxane and boric acid were purchased from Sinopharm Chemical Reagent Co. Ltd, Shanghai, China. CNTs with a diameter of 8–15 nm and length of 3–12 μm were provided by Conductive Materials of Luelida Co. Ltd, Xinxing City, Henan province, China. The fabric used in this study was the plain-woven aramid Kevlar fabric with an areal density of around 200 g m^{-2} [2] and was commercially available. All the chemical reagents were of analytical purity and used as received without further purification.

2.2. Experiments

SSG was prepared by heating dimethyl silicone oil with small amount of pyroboric acid for several hours [32]. 0.3 g CNTs were dispersed in 200 ml mixture solution of alcohol and acetone (1/1, v/v) with 0.06 g SDBS. After stirring for 2 h, 3 g SSG and 0.15 g BPO were added into the CNTs solution and stirred for another 1 h, the mixed solution was then poured into a beaker. The Kevlar fabric was tailored to several specific sizes (11.5 cm \times 11.5 cm, 5 cm \times 5 cm, 10 cm \times 1.5 cm), hung vertically and the mixed CNTs suspension was dripped on the surface of the fabric from top to bottom. The coating

fabric was followed by placing in a 50 °C oven to evaporate the organic solvents. The ‘drip and dry’ process [33] was repeated several times until weight ratio of CNTs to Kevlar was 1:20. Meanwhile, another solution of SSG and BPO with a weight ratio of 20:1 were also prepared in acetone. The same ‘drip and dry’ method was carefully conducted to coat SSG on the surface of CNTs/Kevlar. The weight ratio of SSG/CNTs to Kevlar was kept at 3:5. Finally, the dry SSG/CNTs/Kevlar composites were vulcanized in the oven at 80 °C for 2 h and the S-TENG was obtained by assembling the SSG/CNTs/Kevlar with Cu tape and wires. Additionally, S-TENGs with different weight ratios (1.67% and 5%) of CNTs were also prepared.

2.3. Characterization

The morphology of CNTs/Kevlar and S-TENG were characterized by field emission scanning electron microscopy (FE-SEM, XL30 ESEM). The triboelectric tests were conducted with a vibration system including a signal generator, a power amplifier and an oscillator (JZK-10) (bought from Sino-cera. Piezotronics. INC. China) and the electric output signals were recorded by digital multi-meters (DMM6001). The energy harvesting and safeguarding properties of S-TENGs were explored by drop hammer test systems. And the quasi-static piercing test was conducted on a universal test machine (MTS criterion 43, MTS System Co., America).

3. Results and discussion

3.1. Characterization of S-TENG

The schematic illustration of SSG/CNTs/Kevlar fabrication process was demonstrated in figures 1(a)–(c). CNTs suspension was dripped on the Kevlar surface. After the solvent of suspension was evaporated, SSG was coated on the surface of CNTs/Kevlar in the same way. And the S-TENG was finally obtained by assembling SSG/CNTs/Kevlar with Cu tape and wires. The CNTs layer closed to the Kevlar layer was connected to ground through an external load resistance. The working mechanism for harvesting energy of S-TENG was the coupling effect of contact electrification and electrostatic induction under periodic contact and separation of the two materials [1, 34]. Contact electrification occurred due to the different electron affinities between Kevlar fabric and external material (figure 1(d-1)). Briefly, the Kevlar fabric and external material obtained an equal amount of positive and negative charges after several contact cycles with each other due to their different tribo-polarities. Free electrons flew through the external load due to electrostatic induction (figure 1(d-2)) during the releasing process of the external material. The system turned to electrostatic equilibrium when the external material left far away (figure 1(d-3)). Equivalently, when the external material approached S-TENG again, electrostatic induction drove current in the opposite direction. And the system turned to electrostatic equilibrium again when the Kevlar fabric and the external material were tightly contacted. The corresponding electrical curve of this single-electrode mode S-TENG in one cycle process was demonstrated in figure 1(e). In this way, the

mechanical energy was constantly converted into electricity and the as-prepared S-TENG was enabled to act as a sustainable power source.

SSG exhibited a typical shear stiffening (SS) behavior (figure 2(a)). When the shear frequency was 0.1 Hz, the initial storage modulus (G'_{min}) was 67 Pa, presenting a very soft state. As soon as the shear frequency reached 100 Hz, the maximum storage modulus (G'_{max}) increased 4 orders of magnitude (52 kPa), exhibiting typical SS property. On the other hand, when the shear frequency was under 5 Hz, the storage modulus was lower than the loss modulus (G''), the SSG was macroscopically performed viscous. With the increase of the shear frequency, the storage modulus kept increasing and was higher than the loss modulus, SSG turned from the fluid-like to solid-like status. The sandwich structure of the SSG/CNTs/Kevlar and the schematic illustration of the S-TENG under impact were presented in figures 2(b), (c). The SEM images of the Kevlar fabric with CNTs coated on the surface and the as-prepared SSG/CNTs/Kevlar were shown in figures 2(d)–(g).

Here, the addition of CNTs was to form a conductive layer as well as enhance the mechanic property of the Kevlar. Pristine CNTs were agglomerated with bundles (figure S1a (available online at stacks.iop.org/SMS/29/125007/mmedia)) and SSG could uniformly enter the space of CNTs (figure S1b). Owing to the high visco-elastic characteristic, the addition of SSG guaranteed the mixed CNTs with higher adhering force than pure CNTs. So, the CNTs/SSG were stuck to Kevlar fibers forming a stable conductive layer (figures 2(d), (e)), which endowed its good conductivity (figure 2(h)). Moreover, figures 2(f), (g) displayed the surface and edge microstructures of SSG/CNTs/Kevlar. The final surface of the SSG/CNTs/Kevlar was insulative (figure 2(i)). Based on the above studies, the electrical output performance of the S-TENG with different amounts of CNTs (1.67%, 5%, 6.67%) was explored. And as further increasing the amount of CNTs, the CNTs tended to be agglomerated and easily fell off Kevlar fabric, which was not helpful in fabrication and the stability of S-TENG (figure S2). The test system mainly consisted of S-TENG, oscillator, and force sensor (figure 3(a)). Resistance of the CNTs/Kevlar with 6.67%, 5%, 1.67% CNTs were around 7 k Ω , 100 k Ω , 1500 k Ω , respectively (figure S3). The dependence of the output voltage on the load resistance was measured at the force of 60 N and frequency of 10 Hz by connecting various resistors, ranging from 10³ to 10⁹ Ω to the S-TENG. S-TENGs were kept at 5.5 cm \times 5.5 cm. As shown in figure 3(b), the output voltage and current of S-TENG with 6.67% CNTs varied with different load resistances. The voltage of S-TENG was as low as 0.009 V under 100 k Ω . It started to increase when the resistance was larger than 100 k Ω and finally reached 76.36 V at 1 G Ω . Obviously, the output voltage of S-TENG increased with the increase of loading resistance and the current showed the opposite trend due to Ohm's law (the currents ranged from 8.9 μ A to 0.08 μ A).

The triboelectric properties of S-TENGs with 1.67%, 5% CNTs were also explored at the force of 60 N and frequency of 10 Hz. Voltages of these S-TENGs exhibited similar tendencies to the curve of S-TENG (6.67% CNTs) and the maximum voltage values were respective 58.00 V (figure 3(c))

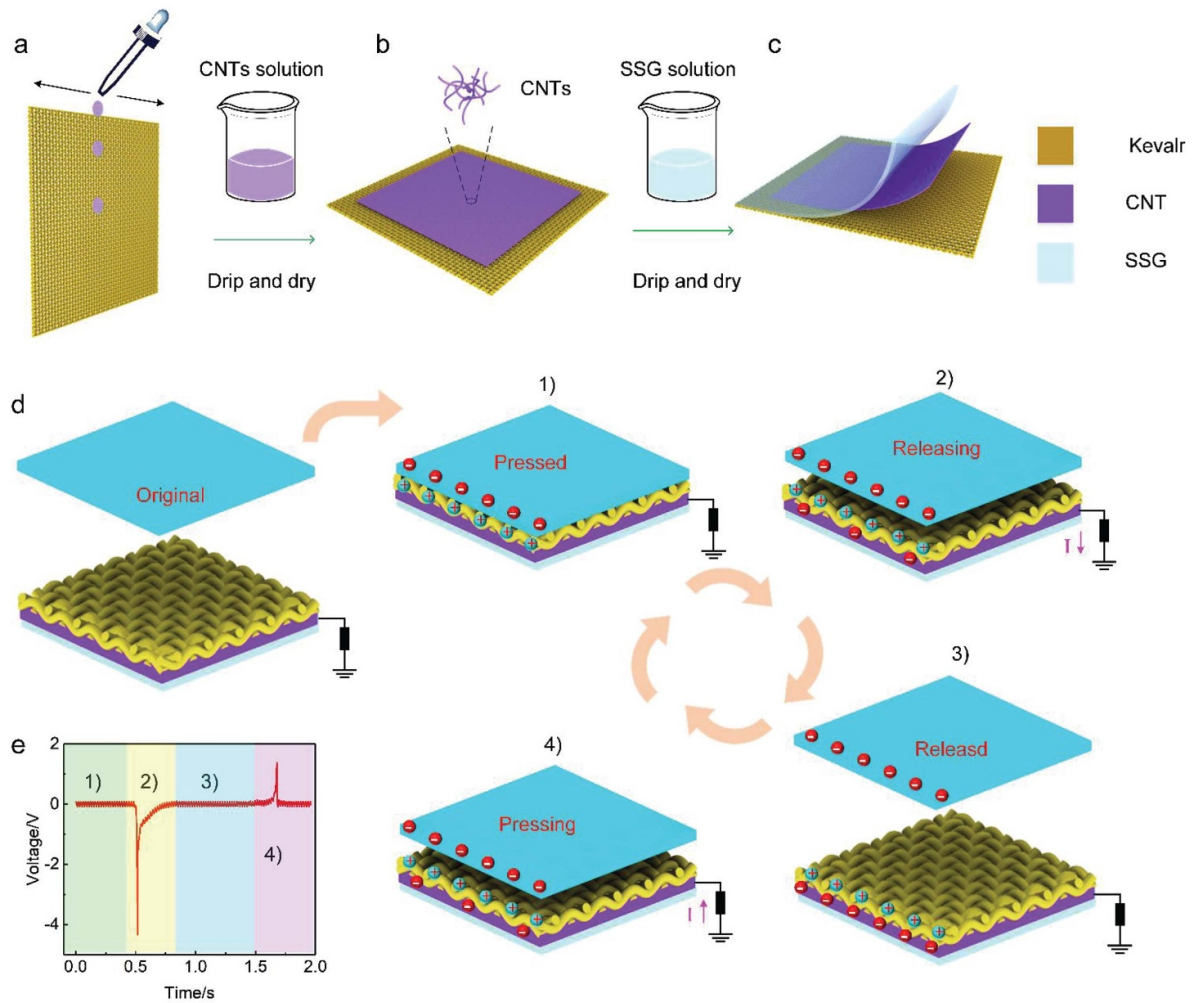


Figure 1. (a)–(c) The schematic illustration of the fabrication process and (d) working mechanism of S-TENG. (e) The output voltage signal in a single release-press process.

and 65.60 V (figure 3(d)). On the other hand, the output power density was further investigated due to its importance for S-TENG. Figure 3(e) exhibited the variations of output power with the load resistance. (Output power was determined by Ohm's law $P = V^2/R$, where P represented power, V was the voltage, R was the load resistance.) The maximum average power of the S-TENG with 6.67% CNTs achieved $212.40 \mu\text{W}$ at the load resistance of $8 \text{ M}\Omega$. The maximum peak power of S-TENG with 5% CNTs was achieved at $134.81 \mu\text{W}$ across $8 \text{ M}\Omega$ resistance (output voltage was 32.84 V). As for S-TENG with 1.67% CNTs, an instantaneous peak power of $105.90 \mu\text{W}$ was obtained at $8 \text{ M}\Omega$. These results demonstrated S-TENG with 6.67% CNTs showed the highest energy-harvesting performance. It was also found that external load resistance also showed a positive influence on the output voltage of S-TENG. This was because when the load resistance was far less than the internal capacitive impedance of S-TENG, the voltage rarely distributed on the load resistance [35]. Reversely, when the load resistance was larger, its impedance was far greater than that of S-TENG which resulted in almost all voltages distributing on the load resistance.

Figure 3(f) demonstrated the output voltages as a function of load resistance of the S-TENG with different amounts of CNTs. The V - Q - x relationship for contact-mode TENG [35, 36] was appropriate to study the triboelectric properties of S-TENGs with different load resistances (V : the voltage between the two electrodes, Q : the amount of transferred charge, x : the separation distance between the two triboelectric charged layers). Based on the theoretical study of the contact-mode TENG [36], a differential equation of the voltage could be expressed by combining the V - Q - x relationship with the Ohm's law as:

$$V(t) = R \frac{dQ}{dt} = V_{OC}(x(t)) - \frac{1}{RC_0} e^{-\frac{t}{RC_0}} \int_0^t V_{OC}(x(t)) e^{\frac{t}{RC_0}} dt \quad (1)$$

V_{OC} was the intercept of the V - Q curve [36], C_0 was the equivalent capacitance of the S-TENG. Given the boundary condition as: $t = 0, x = 0, V = 0$. The relationship between the peak value of voltage and the load resistance during the contact-separation process was obtained (detailed evolution was displayed in supplemental file).

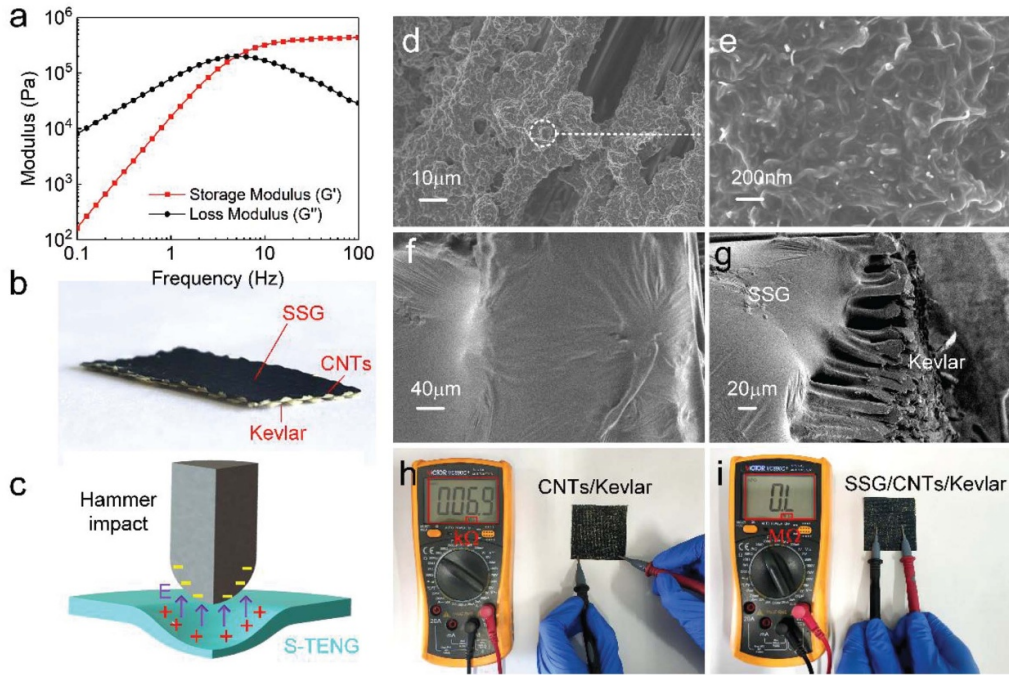


Figure 2. (a) Rheological property of SSG; (b) photo of the three-layer structure; (c) schematic of the triboelectric behavior of S-TENG under impact. (d, e) SEM micrographs of the CNTs/Kevlar and (f, g) the surface and edge of SSG/CNTs/Kevlar, (h) resistance of the CNTs/Kevlar (6.67%) and (i) SSG/CNTs/Kevlar.

$$V_p = V_{OC}(0) e^{-\frac{t_0}{RC_0}} - e^{-\frac{t_0}{RC_0}} \int_0^{t_0} e^{\frac{t}{RC_0}} d(V_{OC}(x(t))) \quad (2)$$

Here, t_0 was the moment that the voltage arrived at the peak value during the contact separation process ($t = t_0$, $V = V_p$). The simplified form of the equation was given as:

$$V_p = Ae^{-\frac{m}{R}} + C \quad (3)$$

where $m = t_0/C_0$, $A = V_{OC}(0)$, C was a constant. The output voltage of S-TENG could be calculated by equation (1).

The peak value of voltage data varied with the load resistance was fitted well by equation (3). The exponent m of S-TENGs with the 6.67%, 5%, 1.67% CNTs were 4.91×10^6 , 5.30×10^6 , 5.44×10^6 , respectively. Meanwhile, the exponent m had a reciprocal relationship with the equivalent capacitance (C_0) of the S-TENG which also implied that the equivalent capacitance increased with the increase of CNT amounts. Detailed analysis of the S-TENG's C_0 was in the supplemental file. The electric conductivity, decreased with the decrease of CNT amounts, also impeded the charges transferred from the primary electrode to the load resistance which further led to a lower output performance [35]. Thus, the high conductivity of the primary electrode exhibited a positive impact on the output property of the S-TENG. Based on the above results, S-TENG with 6.67% CNTs showed the highest efficiency in collecting mechanical energy and as a novel energy source for the following study.

In addition, S-TENGs (6.67% CNTs) exhibited excellent stability which the voltage signals showed no degradation even after 1000 excitations (figure 3(g)) at 8 M Ω . Since fiber-based clothes were often torn in practical activities, the

energy-converting performance of tailed S-TENG was also necessarily studied. The S-TENG (6.67% CNTs) with different sizes and shapes were connected with 8 M Ω resistance and the output voltages were explored (figure 3(h)). Here, we set the sample with size of 5.5 cm \times 5.5 cm as A_0 , the shapes of other tailored S-TENGs were $A_0/3$, $A_0/2$, $2A_0/3$, arrow, cross and heart shape (inset of the figure 3(h)). As shown in figure 3(h), all the cut S-TENGs could also transform mechanical energy into electric energy and the peak values of $A_0/3$, $A_0/2$, $2A_0/3$, A_0 , arrow, cross and heart-shaped S-TENG were 11.1, 18.9, 28.4, 40.9, 25.5, 26.1 and 21.4 V, respectively. The voltages were undoubtedly increased with the increasing contact area of S-TENG. To this end, the as-prepared S-TENG enabled to work as a tailorable energy textile for wearable electronics.

3.2. Self-powered mechanosensing properties

Due to the high flexibility, S-TENG could act as a wearable device to harvest as well as monitor different human motions. Firstly, the S-TENG (10 cm \times 1.5 cm) was attached on the thumb and the output voltages under finger bending motions were recorded. The bending-releasing behavior of the thumb led to the contact and separation between S-TENG and the thumb which generated the output voltage. As shown in figure 4(a), the voltage increased from 0.25 V to 1.37 V with the increase of bending degrees which proved S-TENG could detect different bending states.

Additionally, the S-TENG was also attached on hand to monitor the motions, such as grabbing, pressing, tapping, spitting and touching (figures 4(b), (c)). As displayed in figure

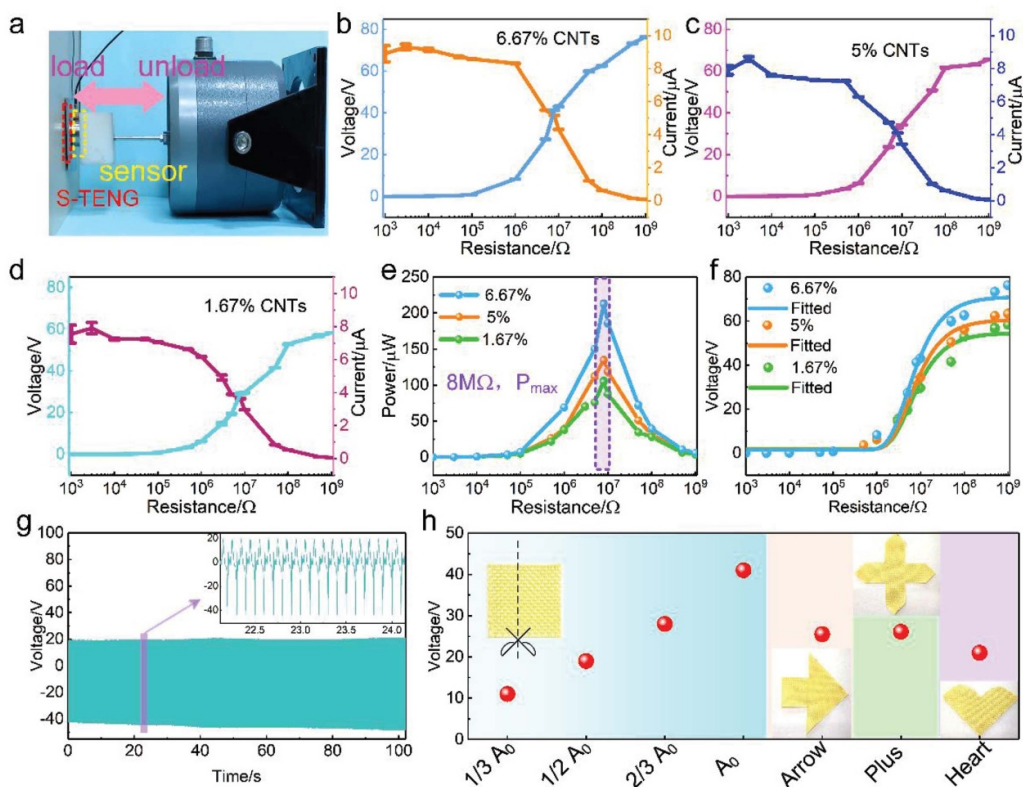


Figure 3. (a) The digital picture of the oscillator test system. (b–e) Voltage, current and output power as a function of load resistance of S-TENG with 6.67%, 5%, 1.67% CNTs; (f) the experimental data and fitting curves of the output voltages of S-TENG with different amounts of CNTs; (g) Stability of S-TENG with 6.67% CNTs at 8 MΩ; (h) peak voltages of the tailorable S-TENG with different sizes and shapes.

4(b), S-TENG was attached to the fingertip, and a pulse voltage signal was immediately generated as the finger pressed PC (Polycarbonate) plate. The subsequent charging signal was kept at zero until the finger left, causing another opposite pulse voltage. The peak values of voltages generated by grabbing, pressing, tapping and spating were around 0.74, 1.83, 3.32 and 12.40 V, respectively. What's more, bent or twisted textile-based S-TENG could normally output varying signals when it was patted by hand (figure S4). These results exhibited that the S-TENG could act as self-powered wearable sensor to detect various thumb motions.

Besides, the S-TENG could also be stuck on fingertip to detect and harvest energy by contacting different materials owing to various triboelectric series [37] between Kevlar and other composites. Once the finger touched external materials (figure 4(d)), S-TENG outputted the charging signals. The biggest voltage value of 0.342 V was generated by touching PC plate (figure 4(e)). To the contrary, the voltage generated by touching the Lyocell fabric (0.070 V) was the smallest. Reliable signals and average values (inset of figure 4(e)) of 0.080, 0.163, 0.250, 0.141, and 0.111 V were presented which corresponded to PDMS, PTEF, Latex, silk, and Cu, respectively.

S-TENGs were further attached on the heel (figure 5(a)) and the waist (figure 5(d)) to sense the contact-separation process of human body movement. The peak values of the output voltage generated by strolling, walking, running and stomping by sticking S-TENG on the heel were around 1.66, 2.19, 2.86

and 5.47 V, respectively (figure 5(b)). Figure 5(c) displayed the changing output voltages under strolling and stomping. Similarly, the output performance of the S-TENG fixed on the waist (figures 5(e), (f)) were also studied. The peak values of the output voltage generated by the contact-separate process between elbow and wrist under walking and running were around 0.98 V and 3.27 V, respectively. In conclusion, the S-TENG as a smart self-powered system could not only harvest energies from body motions, but also monitor these movements as well as distinguish different touching materials which could be applied in wearable self-powered electronic devices and robotic tentacles.

3.3. Sensing and anti-impact properties of S-TENG

Owing to the anti-impact property of Kevlar fabric and the energy dissipation characteristic of SSG, the electric and mechanic performance of the S-TENG under dynamic impact was systematically investigated. Firstly, the as-prepared S-TENG with size of 5 cm × 5 cm was attached on the mobile phone shell. The force hammer and the force sensor were utilized to measure and record the impact force and the penetrating force (figure 6(a)). The pristine mobile phone shell without S-TENG was also tested. As the shell was beaten by hammer, the impact force signal was recorded by piezotronic sensor of the hammer, meanwhile the penetrated force signal was acquired by the charge sensor behind the shell. The protective

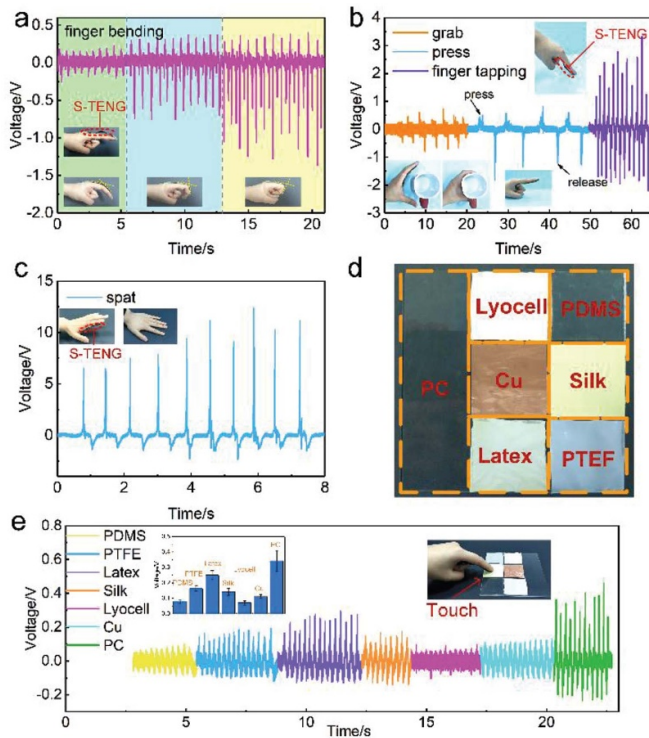


Figure 4. Self-powered force sensing performance of S-TENG under different human motions: (a) finger bending, (b) hand grabbing, pressing, tapping and (c) spatting. (d) Photos of the contacted materials and (e) the corresponding output signals of the S-TENG when they contacted.

performance could be accurately analyzed by comparing the two force signals. As shown in figure 6(c) shells were tested under 130 N and 230 N. For example, when the enhanced shell was under the loading force of 230 N, the maximum penetrated force was 48.7 N, which was smaller than the pristine shell (64.2 N). The charge output signal under hammer impact was simultaneously shown in figure 6(b). The triboelectric voltages under 130 N and 230 N were 0.5 V and 1.2 V, respectively. The voltage generated by high impact force was undoubtedly higher. These results displayed the shell with S-TENG could not only detect impact with variable voltage signals, but also dissipate more impact energy than the pristine shell.

More importantly, the anti-impact experiment on S-TENG (11.5 cm × 11.5 cm) by using the drop hammer machine (figure S5) was further conducted. As shown in figure 6(d), the acceleration sensor was fixed on the mass block and the hammer with the blunt and smooth end was also shown. The acceleration sensor collected the accelerometer signals of impactor and transformed them into electric signals during loading-unloading process. Finally, by using the charge amplifier and oscilloscope, the signals were recorded. The impact energy was controlled by changing drop weight and falling height. Once the impactor loaded from 10 cm on S-TENG, the loading force was immediately increased to maximum and then attenuated to 0 N, followed by rebounding several times until the energy was totally dissipated (figure 6(e)). In addition, as the falling height was 30 cm, the corresponding

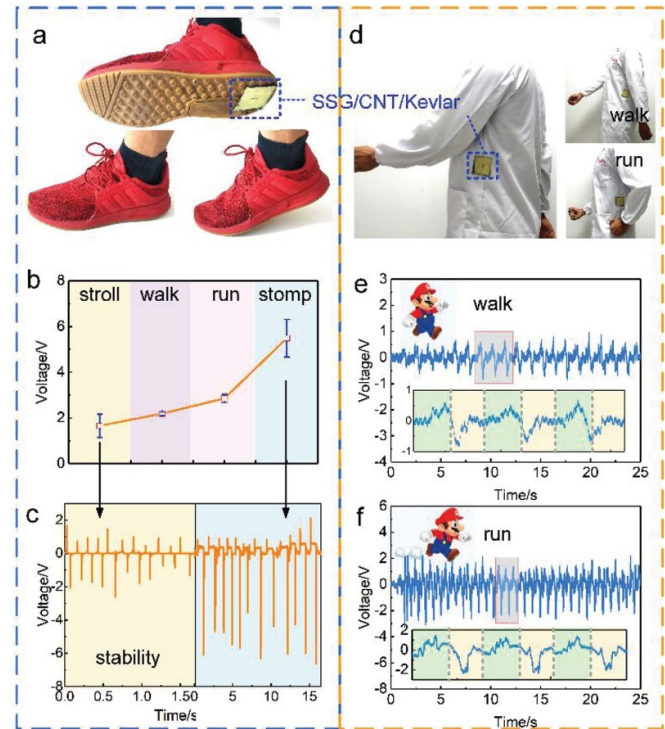


Figure 5. Photographs and sensing performance of S-TENG when attached on (a-c) the heel and (d-f) the waist to monitor the human body movements.

deformations of S-TENGs and neat Kevlar were 5.26 mm and 7.38 mm, respectively (figure 6(f)). The impact force of S-TENG was clearly larger than neat Kevlar while its deformation was smaller which demonstrated the rigidity of S-TENG was higher under dynamic impact (figure 6(g)). Additionally, the slope of S-TENG force-deformation curve was higher than that of Kevlar, which also indicated the equivalent stiffness of S-TENG was increased after introducing SSG. The deformations and force-deformation curves dropped from 10 cm and 20 cm were exhibited similar tendencies (figure S6). Figure 6(h) also compared the deformations of S-TENG and Kevlar under dynamic impact conditions. The result implied that the addition of SSG with the rate-dependent property strengthened the impact resistance performance of Kevlar. Furthermore, the addition of SSG improved the adhesion between Kevlar fibers which was beneficial to disperse the impact force and decrease the deformation. To this purpose, smaller deformation and higher stiffness proved that the S-TENG had a better anti-impact effect compared to the neat Kevlar fabric. On the other hand, the cyclic output voltages, generated by the 1.26 kg impactor fallen from 10, 20 and 30 cm on S-TENG, were around 0.50, 0.80 and 1.50 V, respectively (figure 6(i)). The voltages obviously increased with the increase of impact energy and kept stable over ten loading-unloading excitations. Clearly, S-TENG was capable of resisting and detecting different external harsh impact stimuli. Hence, this novel S-TENG with excellent anti-impact performance and reliable self-powered sensing ability could be used in next generation wearable electronic devices.

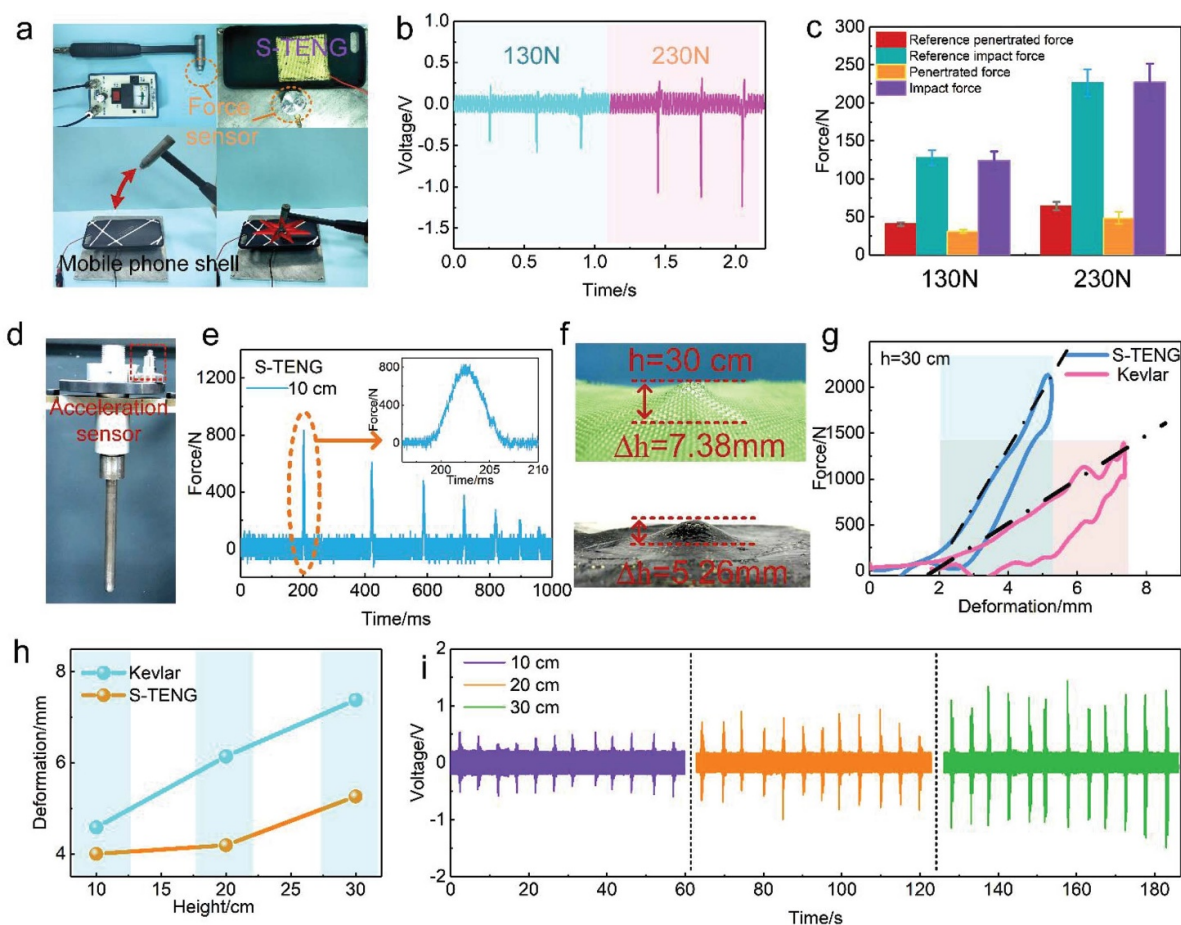


Figure 6. (a) Photographs of the force hammer, the enhanced mobile phone shell with the S-TENG (b) the triboelectric and (c) protective performance of the enhanced mobile phone shell under different impact forces. (d) The equipment of the impactor, (e) the force signal of S-TENG by the impactor falling from 10 cm. (f) Deformations and (g) force-deformation curve of the S-TENG, neat Kevlar under impact from 30 cm. (h) The various deformations of the S-TENG and Kevlar, (i) cyclic triboelectric performance of the S-TENG under the impacts with different falling heights.

The ultimate failure strength of body armor material is vital for determining its lifespan and practical application. So the destruction process of the as-prepared S-TENG under quasi-static puncture and dynamic impact were also necessarily investigated. Firstly, the mechanic and the electric behavior of S-TENG under quasi-static puncture was performed by a needle on MTS with the compression speed of 2 mm min^{-1} (figure 7(a)). During the piercing process, the force value started to increase when the needle contacted the fabric.

It kept increasing with the increase of displacement till the needle totally pierced through the fabric and the force instantaneously decayed from the maximum value of 52.0 N to 0 N. In comparison, the maximum piercing force of neat Kevlar was only 26.3 N, indicating the enhancing mechanical properties of S-TENG. Interestingly, a triboelectric voltage signal could also be observed when the needle pierced through the S-TENG (figure 7(b)).

The mechanical and self-powered sensing properties of S-TENG under harsh impact conditions were further investigated. Here, the mass of the impactor was 3.91 kg. The output voltages and force-deformation curves under high

energy dynamic impact were displayed. As shown in figure 7(c), the areas of force-deformation curves increased with the increasing of falling heights, indicating S-TENG absorbing more kinetic energy. The impact forces of S-TENG under 10, 30, 50 cm impacts were 1418.8 N, 2189.6 N and 2502.4 N, the corresponding deformations were 5.79 mm, 9.89 mm and 14.90 mm, respectively. During the impact from 10 cm to 50 cm, the output voltage was 2.07 V at first and then increased to 4.83 V (figure 7(d), figure S7). These distinguished voltage signals demonstrated S-TENG could be used to monitor external impact excitations.

The impact forces as well as output voltages increased with the increasing of the falling height. Importantly, S-TENG was destroyed under the dropping from 70 cm. The impact forces were firstly increased to maximum and suddenly decreased (figure 7(e)). The impact force of S-TENG increased from 1418.8 N to 2854.3 N with the falling height rising from 10 cm to 70 cm. As for the neat Kevlar, the impact force displayed a similar tendency which increased from 1388.7 N to 1653.4 N as the falling height rising from 10 cm to 30 cm (figure S8, figure 7(e)), and it was entirely lower than the force of

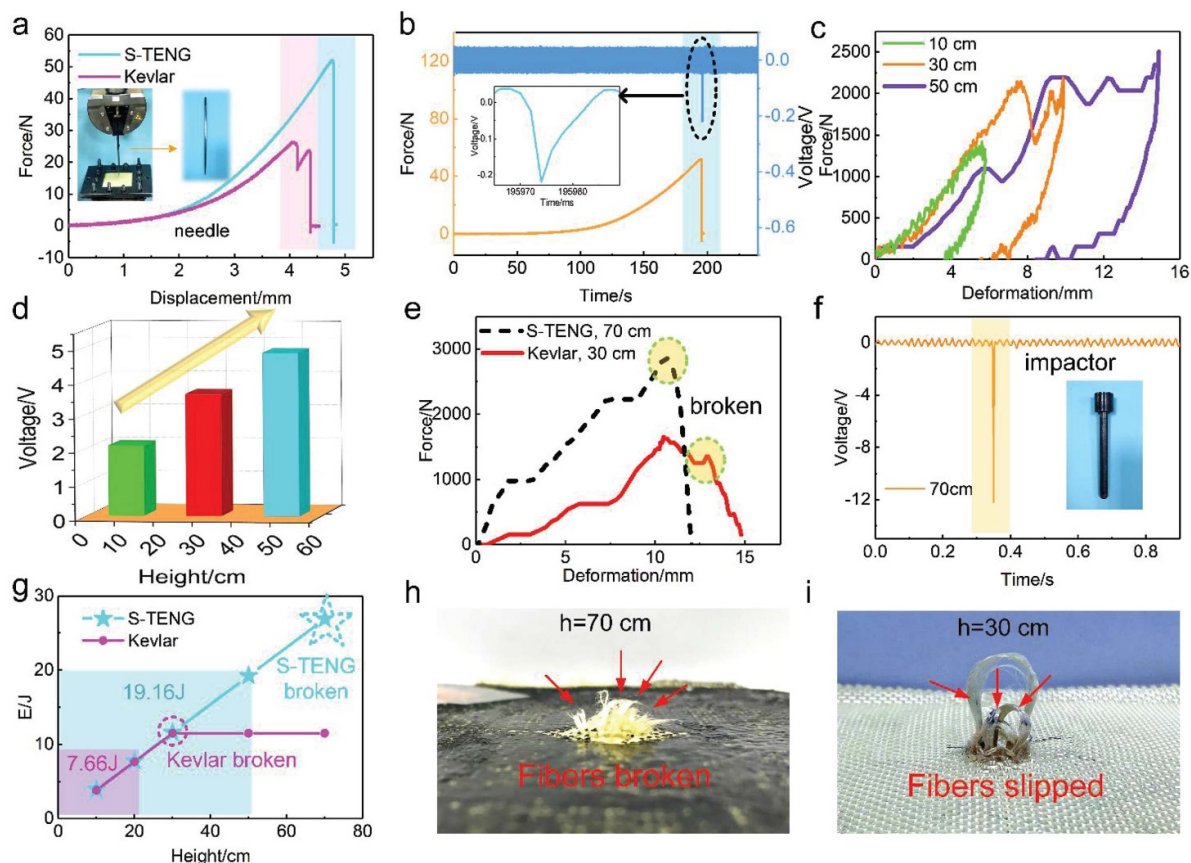


Figure 7. (a) The force-displacement curves of S-TENG and neat Kevlar, (b) electric and the mechanic signals of S-TENG under quasi-static puncture. (c) The force-deformation curves and (d) triboelectric performance under dynamic impact with 3.91 kg impactor. (e) The force signals of S-TENG and Kevlar, (f) voltage signal of S-TENG under destruction. (g) Limited energies that the S-TENG and Kevlar could resist with various falling heights. (h, i) Photos of the destroyed S-TENG and Kevlar.

S-TENG under impact from the same height. Simultaneously, the impact energy ($E = mgh$, m was the impactor mass, g indicated gravity acceleration and h was the falling height) was further calculated. As shown in figure 7(g), the impact energy increased with the increasing of falling heights. The maximum anti-impact energy of neat Kevlar was 7.66 J (falling from 30 cm) and Kevlar was thoroughly broken, slid and penetrated (figure 7(i)). However, S-TENG could resist more dynamic impact energy until it reached 19.16 J (falling from 70 cm). Under these circumstances, fibers of S-TENG were penetrated (figure 7(h)). Besides, the deformations of S-TENG were all smaller than Kevlar under the same impact conditions (figure S9).

These results proved that the S-TENG performed a better anti-impact property compared to Kevlar. It was because the viscoelastic SSG enhanced the adhesion forces between fibers which led to an increase in the stiffness of the composite material. SSG with SS effect also dissipated and resisted kinetic energy under the impact excitations. In conclusion, the fabric-based S-TENG exhibited excellent anti-impact and energy-collecting properties, thus could be utilized in wearable smart electronics as self-powered and safeguarding devices.

4. Conclusion

In this work, a multifunctional flexible S-TENG with enhanced mechanic and good triboelectric performance was fabricated by integrating Kevlar fabric with CNTs and SSG. The wearable S-TENG showed 41.27 V and power of $212.90 \mu\text{W}$ on $8 \text{ M}\Omega$ load resistance at the force and frequency of 60 N and 10 Hz, demonstrating excellent energy-collecting property. CNTs showed a positive influence on the triboelectric performance of S-TENGs. Owing to the excellent triboelectric property, the S-TENG could act as a smart wearable self-powered device to collect and monitor the human motion energy in daily activities. Meanwhile, S-TENG was also capable of distinguishing various contacted materials. Importantly, S-TENG produced an output voltage of 1.50 V as well as decreased the deformation to 71.27% when the 1.26 kg impactor fell from 30 cm, which demonstrated excellent anti-impact performance. Finally, quasi-static and dynamic damage tests were simultaneously studied. This novel S-TENG with self-powered sensing ability could not only gather energies but also resist harsh impacts, showing wide potential in robots, safeguards, wearable electronic devices and human-machine interactions.

Acknowledgments

Financial supports from the National Natural Science Foundation of China (Grant Nos. 11972032, 11802303, 11772320), and China Postdoctoral Science Foundation (Grant Nos. 2018M632543, 2019T120544) are gratefully acknowledged. This study is also supported by the Collaborative Innovation Center of Suzhou Nano Science and Technology.

ORCID iD

Xinglong Gong  <https://orcid.org/0000-0001-6997-9526>

References

- [1] Niu S and Wang Z L 2015 Theoretical systems of triboelectric nanogenerators *Nano Energy* **14** 161–92
- [2] Li S Y, Nie J H, Shi Y X, Tao X L, Wang F, Tian J W, Lin S Q, Chen X Y and Wang Z L 2020 Contributions of different functional groups to contact electrification of polymers *Adv. Mater.* **32** 2001307
- [3] Haque R I and Briand D 2019 Triboelectric freestanding flapping film generator for energy harvesting from gas flow in pipes *Smart Mater. Struct.* **28** 085002
- [4] Xi Y, Guo H Y, Zi Y L, Li X G, Wang J, Deng J N, Li S M, Hu C G, Cao X and Wang Z L 2017 Multifunctional TENG for blue energy scavenging and self-powered wind-speed sensor *Adv. Energy Mater.* **7** 1602397
- [5] Chandrasekhar A, Alluri N R, Vivekananthan V, Purusothaman Y and Kim S J 2017 A sustainable freestanding biomechanical energy harvesting smart backpack as a portable-wearable power source *J. Mater. Chem. C* **5** 1488–93
- [6] Nie J H, Ren Z W, Xu L, Lin S Q, Zhan F, Chen X Y and Wang Z L 2020 Probing contact-electrification-induced electron and ion transfers at a liquid-solid interface *Adv. Mater.* **32** 1905696
- [7] Wang H M, Li D, Zhong W, Xu L, Jiang T and Wang Z L 2019 Self-powered inhomogeneous strain sensor enabled joint motion and three-dimensional muscle sensing *ACS Appl. Mater. Inter.* **11** 34251–7
- [8] Zhu H R, Wang N, Xu Y, Chen S W, Willander M, Cao X and Wang Z L 2016 Triboelectric nanogenerators based on melamine and self-powered high-sensitive sensors for melamine detection *Adv. Funct. Mater.* **26** 3029–35
- [9] Yu X C, Liang X W, Krishnamoorthy R, Jiang W, Zhang L C, Ma L Q, Zhu P L, Hu Y G, Sun R and Wong C P 2020 Transparent and flexible hybrid nanogenerator with welded silver nanowire networks as the electrodes for mechanical energy harvesting and physiological signal monitoring *Smart Mater. Struct.* **29** 045040
- [10] Zhao T M, Zheng C W, He H X, Guan H Y, Zhong T Y, Xing L L and Xue X Y 2019 A self-powered biosensing electronic-skin for real-time sweat Ca²⁺ detection and wireless data transmission *Smart Mater. Struct.* **28** 085015
- [11] Shi Q, Zhang Z, Chen T and Lee C 2019 Minimalist and multi-functional human machine interface (HMI) using a flexible wearable triboelectric patch *Nano Energy* **62** 355–66
- [12] Chandrasekhar A, Alluri N R, Saravanakumar B, Selvarajan S and Kim S J 2016 Human interactive triboelectric nanogenerator as a self-powered smart seat *ACS Appl. Mater. Inter.* **8** 9692–9
- [13] Li S Y, Fan Y, Chen H Q, Nie J H, Liang Y X, Tao X L, Zhang J, Chen X Y, Fu E G and Wang Z L 2020 Manipulating the triboelectric surface charge density of polymers by low-energy helium ion irradiation/implantation *Energy Environ. Sci.* **13** 896–907
- [14] Chen S W, Cao X, Wang N, Ma L, Zhu H R, Willander M, Jie Y and Wang Z L 2017 An ultrathin flexible single-electrode triboelectric-nanogenerator for mechanical energy harvesting and instantaneous force sensing *Adv. Energy Mater.* **7** 1601255
- [15] Mutlu S, Unlu K, Gevrek T N and Sanyal A 2020 Expanding the versatility of poly (dimethylsiloxane) through polymeric modification: an effective approach for improving triboelectric energy harvesting performance *Smart Mater. Struct.* **29** 035024
- [16] Dudem B, Bharat L K, Patnam H, Mule A R and Yu J S 2018 Enhancing the output performance of hybrid nanogenerators based on Al-doped BaTiO₃ composite films: a self-powered utility system for portable electronics *J. Mater. Chem. A* **6** 16101–10
- [17] Zhang H Z, Xia K Q and Fu J M 2019 Pinching a triboelectric nanogenerator using soft pottery for powering electronics *Smart Mater. Struct.* **28** 085036
- [18] Lai Y C, Hsiao Y C, Wu H M and Wang Z L 2019 Waterproof fabric-based multifunctional triboelectric nanogenerator for universally harvesting energy from raindrops, wind, and human motions and as self-powered sensors *Adv. Sci.* **6** 1801883
- [19] Yu A F, Pu X, Wen R M, Liu M M, Zhou T, Zhang K, Zhang Y, Zhai J Y, Hu W G and Wang Z L 2017 Core-shell-yarn-based triboelectric nanogenerator textiles as power cloths *ACS Nano* **11** 12764–71
- [20] Sala de Medeiros M, Chanci D, Moreno C, Goswami D and Martinez R V 2019 Waterproof, breathable, and antibacterial self-powered e-textiles based on omniphobic triboelectric nanogenerators *Adv. Funct. Mater.* **29** 1904350
- [21] Zhang Q, Liang Q, Zhang Z, Kang Z, Liao Q, Ding Y, Ma M, Gao F, Zhao X and Zhang Y 2018 Electromagnetic shielding hybrid nanogenerator for health monitoring and protection *Adv. Funct. Mater.* **28** 1703801
- [22] Kwak S S, Kim H, Seung W, Kim J, Hinchet R and Kim S W 2017 Fully stretchable textile triboelectric nanogenerator with knitted fabric structures *ACS Nano* **11** 10733–41
- [23] Shi M, Wu H, Zhang J, Han M, Meng B and Zhang H 2017 Self-powered wireless smart patch for healthcare monitoring *Nano Energy* **32** 479–87
- [24] Zhu M S, Huang Y, Ng W S, Liu J Y, Wang Z F, Wang Z Y, Hu H and Zhi C Y 2016 3D spacer fabric based multifunctional triboelectric nanogenerator with great feasibility for mechanized large-scale production *Nano Energy* **27** 439–46
- [25] Bunea M, Circiumaru A, Buciumeanu M, Birsan I G and Silva F S 2019 Low velocity impact response of fabric reinforced hybrid composites with stratified filled epoxy matrix *Compos. Sci. Technol.* **169** 242–8
- [26] Khodadadi A, Liaghat G, Bahramian A R, Ahmadi H, Anani Y, Asemani S and Razmkhah O 2019 High velocity impact behavior of Kevlar/rubber and Kevlar/epoxy composites: a comparative study *Compos. Struct.* **216** 159–67
- [27] Majumdar A, Butola B S and Srivastava A 2014 Development of soft composite materials with improved impact resistance using Kevlar fabric and nano-silica based shear thickening fluid *Mater. Design* **54** 295–300
- [28] Malakooti M H, Hwang H S, Goulbourne N C and Sodano H A 2017 Role of ZnO nanowire arrays on the impact response of aramid fabrics *Composites B* **127** 222–31
- [29] Kalman D P, Merrill R L, Wagner N J and Wetzel E D 2009 Effect of particle hardness on the penetration behavior of fabrics intercalated with dry particles and concentrated particle-fluid suspensions *ACS Appl. Mater. Inter.* **1** 2602–12
- [30] Liu M, Zhang S S, Liu S, Cao S S, Wang S, Bai L F, Sang M, Xuan S H, Jiang W Q and Gong X L 2019

- CNT/STF/Kevlar-based wearable electronic textile with excellent anti-impact and sensing performance *Composites A* **126** 105612
- [31] Wang S, Xuan S H, Wang Y P, Xu C H, Mao Y, Liu M, Bai L F, Jiang W Q and Gong X L 2016 Stretchable polyurethane sponge scaffold strengthened shear stiffening polymer and its enhanced safeguarding performance *Acs Appl. Mater. Inter.* **8** 4946–54
- [32] Wang S, Jiang W Q, Jiang W F, Ye F, Mao Y, Xuan S H and Gong X L 2014 Multifunctional polymer composite with excellent shear stiffening performance and magnetorheological effect *J. Mater. Chem. C* **2** 7133–40
- [33] Hu T, Xuan S H, Ding L and Gong X L 2018 Stretchable and magneto-sensitive strain sensor based on silver nanowire-polyurethane sponge enhanced magnetorheological elastomer *Mater. Design* **156** 528–37
- [34] Stanford M G, Li J T, Chyan Y, Wang Z, Wang W and Tour J M 2019 Laser-induced graphene triboelectric nanogenerators *ACS Nano* **13** 7166–74
- [35] Niu S, Wang S, Lin L, Liu Y, Zhou Y S, Hu Y and Wang Z L 2013 Theoretical study of contact-mode triboelectric nanogenerators as an effective power source *Energy Environ. Sci.* **6** 3576–83
- [36] Niu S, Liu Y, Wang S, Lin L, Zhou Y S, Hu Y and Wang Z L 2014 Theoretical investigation and structural optimization of single-electrode triboelectric nanogenerators *Adv. Funct. Mater.* **24** 3332–40
- [37] Liu Z, Li H, Shi B, Fan Y, Wang Z L and Li Z 2019 Wearable and implantable triboelectric nanogenerators *Adv. Funct. Mater.* **29** 1808820